ACADEMIC PRESS

Available online at www.sciencedirect.com

SCIENCE DIRECT®

Journal of Sound and Vibration 270 (2004) 15–38

JOURNAL OF SOUND AND VIBRATION

www.elsevier.com/locate/jsvi

Efficient eigensolution, dynamic response, and eigensensitivity of serpentine belt drives

R.G. Parker*

Department of Mechanical Engineering, The Ohio State University, 206 West 18th ave., Columbus, OH 43210, USA

Received 19 August 2002; accepted 11 February 2003

Abstract

An efficient method for calculating the eigensolutions and dynamic response of a serpentine belt drive is presented. The model is a hybrid discrete-continuous one where the motions consist of rotations of the pulleys, rotation of the tensioner arm, and transverse vibrations of the continuum belt spans adjacent to the tensioner. The speed of solution results from discretization of the belt spans where the unusual feature is the use of Lagrange multipliers to enforce the geometric boundary conditions at the belt-tensioner interface. The method reduces the computational effort by several orders of magnitude compared to published methods using the same model. Also, it is not susceptible to numerical problems that hinder the published methods. The sensitivities of the belt drive natural frequencies to system parameters are also studied. The model parameters under consideration include belt longitudinal stiffness, tensioner spring stiffness, span tensions, belt transport speed, belt density, and pulley moments of inertia. Closed-form expressions for the eigensensitivities to these parameters are obtained using perturbation methods. These expressions are reduced to simple formulae related to the modal strain and kinetic energies. The eigensensitivities are readily determined, quantitatively and qualitatively, by inspection of the modal energy distributions.

1. Introduction

Serpentine belt drives using flat, multi-ribbed belts have largely replaced the older practice of using V-belts to drive individual accessories of an automobile. This system consists of a single belt running over multiple accessory pulleys (Fig. 1). The engine provides the power via a crank-shaft pulley. An important component is the automatic tensioner, which consists of an idler pulley mounted on a spring-loaded tensioner arm. The tensioner maintains proper tension in the belt as the power drawn by accessories and the engine speed change. The advantages of serpentine drives over V-belts include simplified assembly and replacement, longer belt life, compactness, and automatic tension loss compensation.

*Tel.: +1-614-688-3922; fax: +1-614-292-3163.
E-mail address: parker.242@osu.edu (R.G. Parker).

0022-460X/03/$ - see front matter
doi:10.1016/S0022-460X(03)00259-1

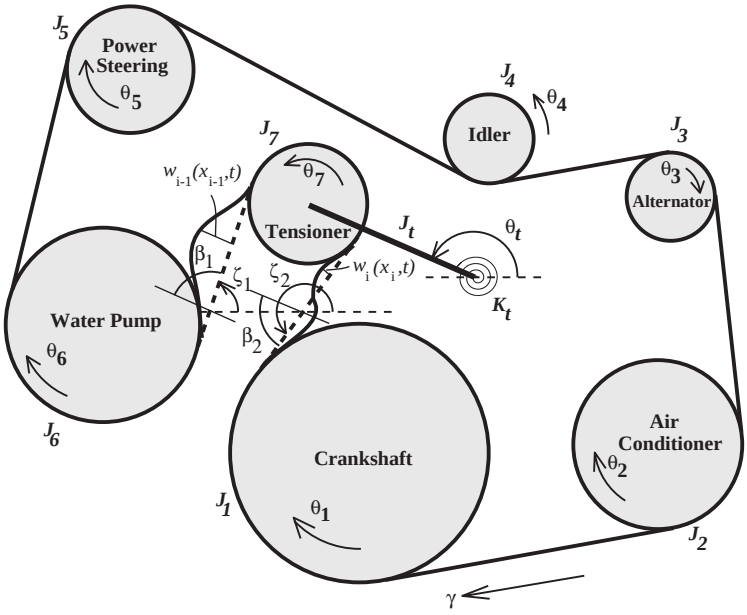

Fig. 1. Serpentine belt drive model.

Two vibratory motions occur in serpentine belt drives: (1) rotational vibration of the accessory pulleys and tensioner arm (with the belt spans acting as axial springs), and (2) transverse vibration of the belt spans. These vibrations cause noise, belt slip, and early failure due to fatigue. Past research breaks into three categories: discrete pulley rotation models with no transverse belt vibration, single belt span models, and coupled belt-pulley models. Using a discrete pulley model, Hawker [1] studied the natural frequencies of damped drive systems with a dynamic tensioner. Barker et al. [2] numerically integrated a similar model to calculate the dynamic response under rapid engine acceleration. Hwang et al. [3] used this model to examine rotational vibration of a serpentine belt drive and used the results to predict the onset of belt slip. Kraver et al. [4] used a similar model to examine tensioner pivot dry friction using an equivalent viscous damper. None of these works include transverse belt span vibrations. Turning to individual belt span modeling, Abrate [5] brought many earlier contributions together in a review article. Subsequently, Ulsoy et al. [6] addressed a parametric instability mechanism capable of causing large lateral belt vibrations due to tension fluctuations. This belt drive instability, also studied by Mockensturm et al. [7], Parker and Lin [8], and Pakdemirli and Ulsoy [9], is addressed using single span models. Beikmann et al. [10] developed a prototypical model consisting of three pulleys and a tensioner arm to study *coupled* belt-pulley vibration. This led to new conclusions regarding linear free vibrations. In particular, results from their model show that coupled belt-pulley vibration modes exist in the frequency range of practical interest. These results point to the importance of coupled belt-pulley modeling for medium and high engine speed regimes. To compute the natural frequencies, Beikmann et al. [10] determine a boundary condition error function and then sweep over a pre-specified frequency range to identify frequencies where the error function vanishes. Zhang and Zu [11] adopted this model to form a continuous system characteristic equation, from which the eigenvalues are calculated by numerical root finding. As discussed later, numerical

problems make both of these methods computationally intensive, prone to errors, and (in the case of the characteristic equation) difficult to generalize to n pulley systems. Furthermore, the resulting eigensolutions are not in a form convenient for use in dynamic response analyses.

The aims of this paper are to present an efficient method to calculate the natural frequencies, vibration modes, and dynamic response of serpentine belt drive systems and to analytically formulate the eigensensitivities to system parameters. The displacements of the spans are represented by a series expansion of basis functions, which leads to a discretization of the kinetic and strain energies for the system. The method presented: (1) is general and works for multiple pulley systems, (2) reduces computation time drastically, (3) reduces errors (missing and false natural frequencies) compared to published methods, and (4) is easily programmed. This work also formulates a simple solution for the eigensensitivity of serpentine belt drive systems. Knowledge of natural frequency sensitivity to system parameters is needed to aid the design and troubleshooting of serpentine drives, which frequently involves tuning natural frequencies to avoid resonant operating conditions. The natural frequency sensitivity is closely related to the modal strain and kinetic energies. This leads naturally to modal strain and kinetic energy diagrams from which the eigensensitivities are readily determined.

2. Mathematical formulation

A prototypical belt-drive system as shown in Fig. 1 consists of n pulleys. The modeling used here is based on the coupled three-pulley, tensioner arm, and belt model developed for constant operating speed [10], although the model here is for n pulleys. This model can be derived from Hamilton's principle following Ref. [10] with straightforward extension to n pulleys. Key assumptions of that model retained in this one are: (1) the belt speed is uniform, (2) belt bending stiffness is negligible, (3) damping is not modeled, and (4) belt-pulley wedging and belt slip at the belt-pulley interfaces are not considered. The non-linear equations of motion for the pulley rotations and transverse belt vibrations are linearized for small transverse belt motions about an operating equilibrium state. The operating equilibrium is determined by an iteration of the non-linear, time-invariant equations as described by Beikmann [12]. This fixes the equilibrium tensioner arm angle and span tensions under steady operating speed and accessory torque loads. For small belt motions, the linearized model decouples the transverse vibration of all belt spans except those adjacent to the tensioner from the pulley rotations. The two spans adjacent to the tensioner remain coupled because tensioner arm rotation induces motion of their endpoints. The result is a hybrid discrete-continuous model where the linearized equations consist of two partial differential equations for the belt spans adjacent to the tensioner and n ordinary differential equations for the $n-1$ driven pulleys and the tensioner arm rotation.

The mathematical model is for a typical system in Fig. 1. Pulley 1 is the driving crank-shaft pulley, and pulleys 2 through n are the driven pulleys. The belt moves clockwise. The system contains a dynamic tensioner, which is restrained at its pivot by an elastic spring, and has pulley i on its free end. θ_j is the rotation of pulley j (taken positive in the direction of belt travel), θ_t is the angular displacement of the tensioner arm (positive counter-clockwise), and $W_j(X,T)$ is the transverse displacement of span j (taken positive for deflection toward the interior of the belt loop). The tensioner pulley rotation θ_i is the absolute rotation, not rotation relative to the tensioner arm.

The equations governing the transverse motion of the belt spans adjacent to the tensioner are

$$\hat{\rho}\frac{\partial^2 W_j}{\partial T^2} - 2\hat{\rho}\hat{\gamma}\frac{\partial^2 W_j}{\partial X \partial T} - (\hat{P}_j - \hat{\rho}\hat{\gamma}^2)\frac{\partial^2 W_j}{\partial X^2} = 0, \quad j = i-1, i, \tag{1}$$

with zero boundary conditions at the endpoints away from the tensioner,

$$W_{i-1}|_0 = 0, \quad W_i|_{\hat{l}_i} = 0. \tag{2}$$

At the span endpoints on the tensioner pulley, the transverse displacement is dictated by tensioner arm rotation:

$$W_{i-1}|_{\hat{l}_{i-1}} = \hat{l}_t\theta_t \cos\beta_1, \quad W_i|_0 = \hat{l}_t\theta_t \cos\beta_2. \tag{3}$$

The equations governing rotation of the pulleys and tensioner arm are

$$\hat{J}_j\ddot{\theta}_j + \hat{k}_j\hat{R}_j(\hat{R}_j\theta_j - \hat{R}_{j+1}\theta_{j+1}) - \hat{k}_{j-1}\hat{R}_j(\hat{R}_{j-1}\theta_{j-1} - \hat{R}_j\theta_j) = \hat{M}_j,$$
$$j = 2, \ldots, n, \quad j \neq i-1, i, i+1; \tag{4}$$

$$\hat{J}_{i-1}\ddot{\theta}_{i-1} + \hat{k}_{i-1}\hat{R}_{i-1}(\hat{R}_{i-1}\theta_{i-1} - \hat{R}_i\theta_i - \hat{l}_t\theta_t \sin\beta_1) - \hat{k}_{i-2}\hat{R}_{i-1}(\hat{R}_{i-2}\theta_{i-2} - \hat{R}_{i-1}\theta_{i-1}) = \hat{M}_{i-1},$$
$$i \neq 2, \tag{5}$$

$$\hat{J}_i\ddot{\theta}_i + \hat{k}_i\hat{R}_i(\hat{R}_i\theta_i - \hat{R}_{i+1}\theta_{i+1} + \hat{l}_t\theta_t \sin\beta_2) - \hat{k}_{i-1}\hat{R}_i(\hat{R}_{i-1}\theta_{i-1} - \hat{R}_i\theta_i - \hat{l}_t\theta_t \sin\beta_1) = \hat{M}_i, \tag{6}$$

$$\hat{J}_{i+1}\ddot{\theta}_{i+1} + \hat{k}_{i+1}\hat{R}_{i+1}(\hat{R}_{i+1}\theta_{i+1} - \hat{R}_{i+2}\theta_{i+2}) - \hat{k}_i\hat{R}_{i+1}(\hat{R}_i\theta_i - \hat{R}_{i+1}\theta_{i+1} + \hat{l}_t\theta_t \sin\beta_2) = \hat{M}_{i+1}, \quad i \neq n, \tag{7}$$

$$\begin{aligned}
&\hat{J}_t\ddot{\theta}_t + [\hat{k}_t\hat{l}_t + \hat{k}_{i-1}\hat{l}_t \sin^2\beta_1 + \hat{k}_i\hat{l}_t \sin^2\beta_2]\hat{l}_t\theta_t - \hat{k}_{i-1}\hat{l}_t(\hat{R}_{i-1}\theta_{i-1} - \hat{R}_i\theta_i)\sin\beta_1 \\
&+ \hat{k}_i\hat{l}_t(\hat{R}_i\theta_i - \hat{R}_{i+1}\theta_{i+1})\sin\beta_2 + \hat{\rho}\hat{\gamma}\hat{l}_t\left(\left.\frac{\partial W_{i-1}}{\partial T}\right|_{\hat{l}_{i-1}} \cos\beta_1 - \left.\frac{\partial W_i}{\partial T}\right|_0 \cos\beta_2\right) \\
&+ (\hat{P}_{i-1} - \hat{\rho}\hat{\gamma}^2)\hat{l}_t\left.\frac{\partial W_{i-1}}{\partial X}\right|_{\hat{l}_{i-1}} \cos\beta_1 - (\hat{P}_i - \hat{\rho}\hat{\gamma}^2)\hat{l}_t\left.\frac{\partial W_i}{\partial X}\right|_0 \cos\beta_2 = 0,
\end{aligned} \tag{8}$$

where $\hat{J}_t = \hat{J}_{arm} + \hat{m}_i\hat{l}_t^2$; $\hat{m}_i$ is the mass of the tensioner pulley; i denotes the tensioner pulley; $\hat{k}_j = EA/\hat{l}_j$; $\hat{\gamma}$ is the uniform belt transport speed; $\hat{\rho}$ is the belt mass per unit length; EA denotes the longitudinal belt stiffness; $\hat{P}_j$ is the equilibrium tension in span j; $\hat{l}_j$ is the length of span j; $\hat{R}_j$ are the pulley radii; $\hat{J}_j$ are pulley moments of inertia; $\hat{l}_t$ is the tensioner arm length; $\hat{K}_r = \hat{k}_t\hat{l}_t^2$ is the tensioner rotational spring stiffness; $\hat{M}_j(T)$ are moments applied by the driven accessories (with steady, average moments being negative); and $\beta_{1,2}$ are the tensioner arm alignment angles at equilibrium given by $\beta_{1,2} = (\theta_t - \zeta_{1,2})_{equil}$, where $\zeta_{1,2}$ are the tensioner span inclination angles from the horizontal to the *exterior* of the belt loop (Fig. 1).

The convention $\theta_{n+1} = \theta_1$ is adopted. The crank-shaft rotation θ_1 drives the system; it is dictated by the engine firing pulses and assumed to be a specified function of time. Typically it is modeled as harmonic or periodic excitation at the firing frequency.

The pulley angular rotations θ_j are defined in terms of new co-ordinates ϕ_j according to

$$\hat{R}_j\theta_j = \hat{R}_1\theta_1 - \hat{R}_1\phi_j \Rightarrow \phi_j = \theta_1 - \frac{\hat{R}_j\theta_j}{\hat{R}_1} \tag{9}$$

with the consequence that $\phi_1 = \phi_{n+1} = 0$. The dimensionless parameters of the system are

$$l_t = \frac{\hat{l}_t}{\hat{R}_1},\ \ l_j = \frac{\hat{l}_t}{\hat{l}_1},\ \ w_j = \frac{W_j}{\hat{R}_1},\ \ x_j = \frac{X_j}{\hat{l}_1},\ \ R_1 = \frac{\hat{R}_1}{\hat{l}_1},\ \ \gamma = \frac{\hat{\gamma}}{\sqrt{\hat{P}_1/\hat{\rho}}},\ \ t = \frac{T}{\sqrt{\hat{\rho}\hat{l}_1^2/\hat{P}_1}}$$

$$P_j = \frac{\hat{P}_j}{\hat{P}_1},\ \ k_b = \frac{EA}{\hat{P}_1},\ \ k_j = \frac{\hat{l}_1\hat{k}_j}{\hat{P}_1} = \frac{k_b}{l_j},\ \ k_t = \frac{\hat{l}_1\hat{k}_t}{\hat{P}_1},\ \ J_t = \frac{\hat{J}_t}{\hat{\rho}\hat{l}_1\hat{R}_1^2},\ \ J_j = \frac{\hat{J}_j}{\hat{\rho}\hat{l}_1\hat{R}_j^2},$$

$$M_j = \frac{\hat{M}_j}{(\hat{P}_1\hat{R}_j\hat{R}_1/\hat{l}_1)}. \tag{10}$$

In dimensionless form, the governing equations are

$$\frac{\partial^2 w_j}{\partial t^2} - 2\gamma\frac{\partial^2 w_j}{\partial x_j \partial t} - (P_j - \gamma^2)\frac{\partial^2 w_j}{\partial x_j^2} = 0,\ \ j = i-1, i, \tag{11}$$

$$w_{i-1}|_0 = 0,\ \ w_i|_{l_i} = 0, \tag{12}$$

$$w_{i-1}|_{l_{i-1}} = l_t\theta_t\cos\beta_1,\ \ w_i|_0 = l_t\theta_t\cos\beta_2, \tag{13}$$

$$J_j\ddot{\phi}_j + \frac{k_b}{l_j}(\phi_j - \phi_{j+1}) - \frac{k_b}{l_{j-1}}(\phi_{j-1} - \phi_j) = J_j\ddot{\theta}_1 - M_j,\quad j = 2, \ldots, n, j \neq i-1, i, i+1, \tag{14}$$

$$\begin{aligned} &J_{i-1}\ddot{\phi}_{i-1} + \frac{k_b}{l_{i-1}}(\phi_{i-1} - \phi_i + l_t\theta_t\sin\beta_1) - \frac{k_b}{l_{i-2}}(\phi_{i-2} - \phi_{i-1}) \\ &\quad = J_{i-1}\ddot{\theta}_1 - M_{i-1},\quad i \neq 2, \end{aligned} \tag{15}$$

$$J_i\ddot{\phi}_i + \frac{k_b}{l_i}(\phi_i - \phi_{i+1} - l_t\theta_t\sin\beta_2) - \frac{k_b}{l_{i-1}}(\phi_{i-1} - \phi_i + l_t\theta_t\sin\beta_1) = J_i\ddot{\theta}_1, \tag{16}$$

$$J_{i+1}\ddot{\phi}_{i+1} + \frac{k_b}{l_{i+1}}(\phi_{i+1} - \phi_{i+2}) - \frac{k_b}{l_i}(\phi_i - \phi_{i+1} - l_t\theta_t\sin\beta_2) = J_{i+1}\ddot{\theta}_1 - M_{i+1}, i \neq n, \tag{17}$$

$$\begin{aligned} &J_t\ddot{\theta}_t + (k_t + \frac{k_b}{l_{i-1}}\sin^2\beta_1 + \frac{k_b}{l_i}\sin^2\beta_2)l_t^2\theta_t \\ &\quad - \frac{k_b}{l_{i-1}}l_t(\phi_i - \phi_{i-1})\sin\beta_1 + \frac{k_b}{l_i}l_t(\phi_{i+1} - \phi_i)\sin\beta_2 \\ &\quad + \gamma l_t(\left.\frac{\partial w_{i-1}}{\partial t}\right|_{l_{i-1}}\cos\beta_1 - \left.\frac{\partial w_i}{\partial t}\right|_0\cos\beta_2) \\ &\quad + (P_{i-1} - \gamma^2)l_t\left.\frac{\partial w_{i-1}}{\partial x_{i-1}}\right|_{l_{i-1}}\cos\beta_1 - (P_i - \gamma^2)l_t\left.\frac{\partial w_i}{\partial x_i}\right|_0\cos\beta_2 = 0. \end{aligned} \tag{18}$$

Eqs. (11)–(18) can be given an extended operator form to provide mathematical structure that allows natural use of classical methods of analysis. The extended variable a representing the

system displacements is defined as

$$a = \left\{ \underbrace{w_{i-1}, w_i}_{spans}, \underbrace{\phi_2, \ldots, \phi_j, \ldots, \phi_{i-1}, \phi_i, \phi_{i+1}, \ldots, \phi_n}_{pulleys}, \underbrace{\theta_t}_{tensioner} \right\}^{\mathrm{T}}. \tag{19}$$

Note that, in addition to pulley and tensioner rotations, a includes the continuum deflections of the two tensioner spans. With the extended operators M, G, K and $\tilde{K}$ acting on the extended variable a, the equations above are compactly written as

$$Ma_{tt} - Ga_t + (K - \gamma^2 \tilde{K})a = f, \tag{20}$$

$$Ma = \left(w_{i-1}, w_i, J_2\phi_2, ..., J_n\phi_n, J_t\theta_t\right)^{\mathrm{T}}, \tag{21}$$

$$Ga = \left(2\gamma \frac{\partial w_{i-1}}{\partial x_{i-1}}, 2\gamma \frac{\partial w_i}{\partial x_i}, \underbrace{0, \ldots, 0}_{n-1}, \gamma l_t w_i|_0 \cos\beta_2 - \gamma l_t w_{i-1}|_{l_{i-1}} \cos\beta_1 \right)^{\mathrm{T}}, \tag{22}$$

$$Ka = \begin{pmatrix} -P_{i-1}\dfrac{\partial^2 w_{i-1}}{\partial x_{i-1}^2} \\ -P_i \dfrac{\partial^2 w_i}{\partial x_i^2} \\ \left(\dfrac{k_b}{l_2} + \dfrac{k_b}{l_1}\right)\phi_2 - \dfrac{k_b}{l_2}\phi_3 \\ \vdots \\ -\dfrac{k_b}{l_{j-1}}\phi_{j-1} + \left(\dfrac{k_b}{l_j} + \dfrac{k_b}{l_{j-1}}\right)\phi_j - \dfrac{k_b}{l_j}\phi_{j+1} \\ \vdots \\ -\dfrac{k_b}{l_{i-2}}\phi_{i-2} + \left(\dfrac{k_b}{l_{i-1}} + \dfrac{k_b}{l_{i-2}}\right)\phi_{i-1} - \dfrac{k_b}{l_{i-1}}\phi_i + \dfrac{k_b}{l_{i-1}} l_t\theta_t \sin\beta_1 \\ -\dfrac{k_b}{l_{i-1}}\phi_{i-1} + \left(\dfrac{k_b}{l_i} + \dfrac{k_b}{l_{i-1}}\right)\phi_i - \dfrac{k_b}{l_i}\phi_{i+1} - \left(\dfrac{k_b}{l_{i-1}}\sin\beta_1 + \dfrac{k_b}{l_i}\sin\beta_2\right) l_t\theta_t \\ -\dfrac{k_b}{l_i}\phi_i + \left(\dfrac{k_b}{l_{i+1}} + \dfrac{k_b}{l_i}\right)\phi_{i+1} - \dfrac{k_b}{l_{i+1}}\phi_{i+2} + \dfrac{k_b}{l_i} l_t\theta_t \sin\beta_2 \\ \vdots \\ -\dfrac{k_b}{l_{n-1}}\phi_{n-1} + \left(\dfrac{k_b}{l_n} + \dfrac{k_b}{l_{n-1}}\right)\phi_n \\ \left[\left(k_t + \dfrac{k_b}{l_{i-1}}\sin^2\beta_1 + \dfrac{k_b}{l_i}\sin^2\beta_2\right) l_t^2\theta_t + P_{i-1} l_t \left.\dfrac{\partial w_{i-1}}{\partial x_{i-1}}\right|_{l_{i-1}} \cos\beta_1 - P_i l_t \left.\dfrac{\partial w_i}{\partial x_i}\right|_0 \cos\beta_2 \right. \\ \left. -\dfrac{k_b}{l_{i-1}} l_t(\phi_i - \phi_{i-1})\sin\beta_1 + \dfrac{k_b}{l_i} l_t(\phi_{i+1} - \phi_i)\sin\beta_2 \right] \end{pmatrix}, \tag{23}$$

$$\tilde{K}a = \left(-\frac{\partial^2 w_{i-1}}{\partial x_{i-1}^2}, -\frac{\partial^2 w_i}{\partial x_i^2}, \underbrace{0, \ldots, 0}_{n-1}, l_t \frac{\partial w_{i-1}}{\partial x_{i-1}}\bigg|_{l_{i-1}} \cos\beta_1 - l_t \frac{\partial w_i}{\partial x_i}\bigg|_0 \cos\beta_2 \right)^{\mathrm{T}}, \tag{24}$$

$$f = (0, 0, J_2\ddot{\theta}_1 - M_2, \cdots, J_n\ddot{\theta}_1 - M_n, 0)^{\mathrm{T}}. \tag{25}$$

The inner product between two extended variables y and z is defined as

$$\langle y, z \rangle = \int_0^{l_{i-1}} y_1 \bar{z}_1 \, \mathrm{d}x_{i-1} + \int_0^{l_i} y_2 \bar{z}_2 \, \mathrm{d}x_i + y_3 \bar{z}_3 + \cdots + y_{n+2} \bar{z}_{n+2}, \tag{26}$$

where y_r and z_r are elements of the extended variables y and z and the overbar indicates the complex conjugate. With this inner product, the operators M, K, and $\tilde{K}$ are self-adjoint while G is skew self-adjoint; M and K are positive-definite while $\tilde{K}$ is positive semi-definite; and, the space of extended variables having the form (19) is a Hilbert space. This structure is essential for application of perturbation, weighted residual, averaging, and other methods. Examples exploiting this mathematical structure to apply classical analysis techniques for this system and similar discrete-continuous ones are given in Beikmann et al. [13], Zhang and Zu [11], Parker [14], and Parker and Mote [15].

The separable solution form $a \to ae^{\mathrm{i}\omega t}$ yields the eigenvalue problem

$$-\omega^2 Ma - \mathrm{i}\omega Ga + La = 0, \tag{27}$$

where $L = K - \gamma^2 \tilde{K}$. The component equations of this eigenvalue problem are obtained from Eqs. (11)–(18) by assuming all elements of a have separable time dependence of the form $e^{\mathrm{i}\omega t}$. The dimensionless natural frequencies ω are related to the dimensional ones by $\hat{\omega} = \omega\sqrt{\hat{P}_1/\hat{\rho}\hat{l}_1^2}$.

3. Discretization of the continuum belt spans

The motivation for an efficient discretization method lies in the numerical difficulties and computational effort required of prior eigensolutions methods. Two eigensolution methods based on the present belt-pulley modeling have been proposed in the literature. Both retain the continuum belt model and rely on searching for roots of characteristic equations. Beikmann et al. [10] established a two-loop iteration process. For a candidate ω, the first loop calculates the pulley rotations and span tensions. With these known, the second loop uses three of the four belt boundary conditions and the tensioner equation of motion to determine the span deflections. The error in the fourth boundary condition is evaluated; if it is zero then ω is a natural frequency, otherwise ω is incremented and the process repeated. Zhang and Zu [11] studied the same three-pulley system and produced a closed-form expression for the characteristic equation. This method is simpler to program but has the drawback that it does not readily generalize to systems with an arbitrary number of pulleys. In both methods, the natural frequencies are determined by seeking roots of a characteristic equation over a *pre-specified* frequency range. Characteristic equations are notoriously ill behaved numerically, and root finding methods generally have difficulty beyond the first few natural frequencies. To visualize this problem, a typical error function using Beikmann's method is shown in Fig. 2(a) for a seven-pulley example, while Fig. 2(b) exhibits the

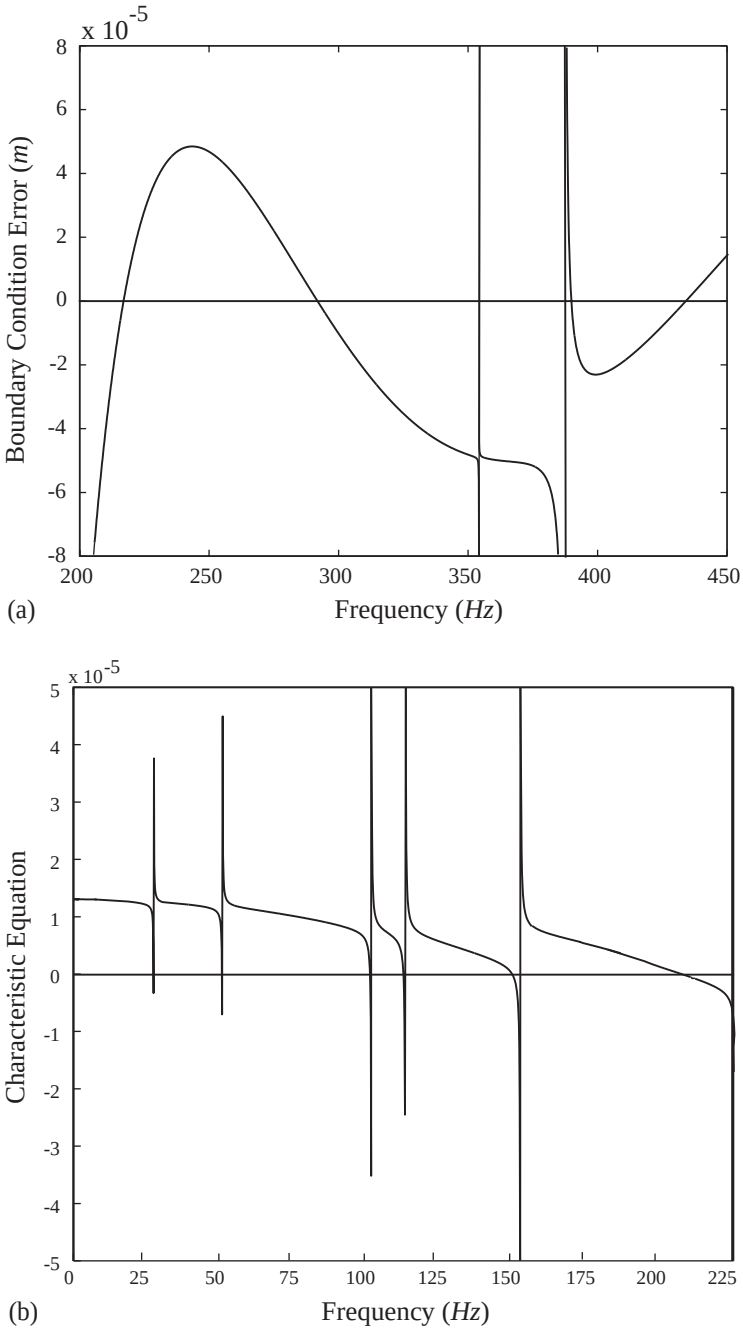

Fig. 2. Typical error functions for the numerical eigensolution procedure developed in (a) Beikmann et al. [10] and (b) Zhang and Zu [11].

characteristic equation for the 3-pulley example system used by Zhang and Zu. Even state-of-the-art root finding algorithms applied to such functions can lead to missing roots, erroneous calculation of two roots where only one exists, and expensive computation in narrowing the frequency resolution to resolve these issues, which are problem dependent. We consistently encountered these problems for a variety of automotive drives in practical use. Furthermore, one needs to specify the frequency search range a priori, though it may not be well known. Once found, the continuum vibration modes are cumbersome for dynamic response analyses. A more robust, problem-independent approach is required to reliably predict the eigensolutions and dynamic response.

With the extended operator formulation (20) and associated inner product (26) the hybrid discrete-continuous system is in principle amenable to weighted residual methods such as Galerkin discretization (see Refs. [13,14]). Such global discretizations require that admissible functions Θ_j in expansions of the extended variable as $a = \sum_{j=1}^{m} c_j(t)\Theta_j$ be from the space of extended variables that describe an overall deflection of the entire belt drive (pulley/tensioner rotations and span deflections). These must satisfy the boundary conditions (13) at the span tensioner interface. There is no clear way to identify suitable extended admissible functions that are complete and efficiently describe the motion. Consequently, a *local* discretization of only the two spans adjacent to the tensioner is adopted.

The deflections of the two spans adjacent to the tensioner are expanded in series of basis functions as

$$w_{i-1}(\xi_{i-1}, t) = \sum_{r=1}^{f} a_r(t)\alpha_r(\xi_{i-1}),$$
$$w_i(\xi_i, t) = \sum_{r=1}^{f} b_r(t)\psi_r(\xi_i), \tag{28}$$

where $\xi_{i-1} = x_{i-1}/l_{i-1}$, $\xi_i = x_i/l_i$, and α_r and ψ_r are non-dimensional basis functions that satisfy zero boundary conditions at the bounding points away from the tensioner ($\alpha_r(0) = 0, \psi_r(1) = 0$). The α_r and ψ_r are *not* constrained by any boundary conditions at the span endpoints on the tensioner. The geometric boundary conditions (13) will be enforced subsequently as constraints.

The chosen basis functions are orthonormal polynomials determined by $\int_0^1 \alpha_r\alpha_s \,\mathrm{d}\xi_{i-1} = \delta_{rs}$, $\int_0^1 \psi_r\psi_s \,\mathrm{d}\xi_i = \delta_{rs}$. These are conveniently represented in terms of the orthogonal polynomials $\eta_m(\xi)$ with $\int_0^1 \eta_r(\xi)\eta_s(\xi)\,\mathrm{d}\xi = 1$ as

$$\alpha_m(\xi_{i-1}) = \eta_m(\xi_{i-1})/\sqrt{l_{i-1}},$$
$$\psi_m(\xi_i) = \eta_m(1-\xi_i)/\sqrt{l_i}. \tag{29}$$

The first four $\eta_m(\xi)$ are (Fig. 3)

$$\eta_1(\xi) = \sqrt{3}\xi, \quad \eta_2(\xi) = 4\sqrt{5}(\xi^2 - 3/4\xi),$$
$$\eta_3(\xi) = 15\sqrt{7}(\xi^3 - 4/3\xi^2 + 2/5\xi),$$
$$\eta_4(\xi) = 168(\xi^4 - 15/8\xi^3 + 15/14\xi^2 - 5/28\xi).$$

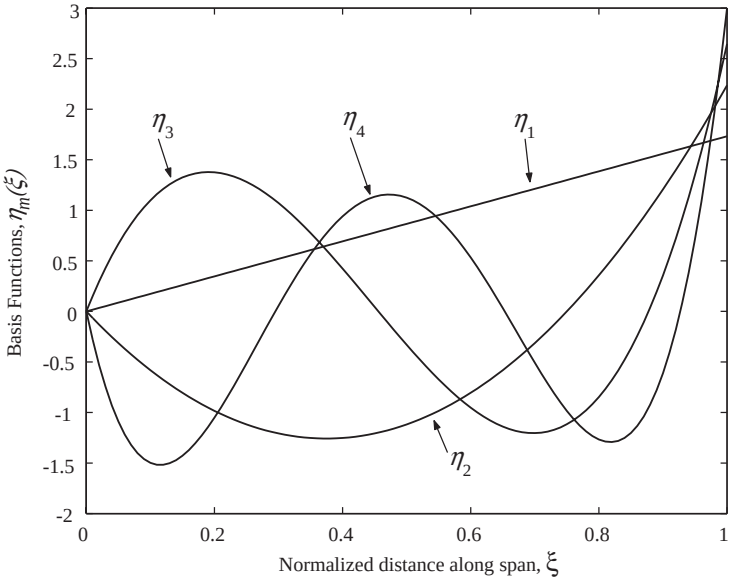

Fig. 3. Basis functions $\eta_m(\xi)$ for series expansion of belt deflections.

The non-dimensional kinetic and strain energies are

$$T = \frac{\hat{T}}{(\hat{P}_1\hat{R}_1^2)/\hat{l}_1} = \sum_{j=2}^{n}\frac{1}{2}J_j(\dot{\phi}_j - \dot{\theta}_1)^2 + \frac{1}{2}J_t\dot{\theta}_t^2 + \sum_{s=i-1}^{i}\frac{1}{2}\int_0^{l_s}\left(\frac{\partial w_s}{\partial t} - \gamma\frac{\partial w_s}{\partial x_s}\right)^2 \mathrm{d}x_s = \sum_{j=2}^{n} T_j + T_t + T_{span}^{i-1} + T_{span}^{i}, \tag{30}$$

$$V = \frac{\hat{V}}{(\hat{P}_1\hat{R}_1^2)/\hat{l}_1} = \sum_{j=1 j\neq i-1,i}^{n}\frac{1}{2}\frac{k_b}{l_j}(\phi_{j+1} - \phi_j)^2 + \frac{1}{2}\frac{k_b}{l_{i-1}}(\phi_i - \phi_{i-1} - l_t\theta_t\sin\beta_1)^2 + \frac{1}{2}\frac{k_b}{l_i}(\phi_{i+1} - \phi_i + l_t\theta_t\sin\beta_2)^2 + \frac{1}{2}k_t l_t^2\theta_t^2 + \sum_{s=i-1}^{i}\frac{1}{2}\int_0^{l_s} P_s\left(\frac{\partial w_s}{\partial x_s}\right)^2 \mathrm{d}x_s = V_{stretch} + V_t + V_{span}^{i-1} + V_{span}^{i}. \tag{31}$$

Introducing the unknown Lagrange multipliers λ_1 and λ_2, the dimensionless Lagrange's equations are

$$\ell = T - V,$$
$$\frac{\mathrm{d}}{\mathrm{d}t}\left(\frac{\partial \ell}{\partial \dot{q}_s}\right) - \frac{\partial \ell}{\partial q_s} = \lambda_1 A_{1s} + \lambda_2 A_{2s}, s = 1, 2, \ldots, 2f + n, \tag{32}$$

λ_1 and λ_2 are the dimensionless boundary forces required to enforce the boundary conditions at the tensioner end of the spans. The holonomic constraints on the generalized co-ordinates $a_r(t)$, $b_r(t)$, and $\theta_t(t)$ come from the boundary conditions (13)

$$\begin{aligned} \Phi_1 &= w_{i-1}|_{l_{i-1}} - l_t\theta_t\cos\beta_1 = \textstyle\sum_{r=1}^{f} a_r(t)\alpha_r(1) - l_t\theta_t\cos\beta_1 = 0, \\ \Phi_2 &= w_i|_0 - l_t\theta_t\cos\beta_2 = \textstyle\sum_{r=1}^{f} b_r(t)\psi_r(0) - l_t\theta_t\cos\beta_2 = 0. \end{aligned} \tag{33}$$

The $A_{1s} = \partial\Phi_1/\partial q_s$ and $A_{2s} = \partial\Phi_2/\partial q_s$ in Eq. (32) are the coefficients of the sth generalized co-ordinate in the constraints Φ_1 and Φ_2, respectively, where the generalized co-ordinates q_s are ordered as $a_1, \ldots a_f, b_1, \ldots b_f, \phi_2, \ldots, \phi_n, \theta_t$. Thus,

$$\left.\begin{matrix} A_{1s} = \alpha_s(1) \\ A_{2s} = 0 \end{matrix}\right\} \; s = 1, 2, \ldots, f, \quad \left.\begin{matrix} A_{1s} = 0 \\ A_{2s} = \psi_s(0) \end{matrix}\right\} \; s = f+1,\ f+2, \ldots 2f,$$

$$\left.\begin{matrix} A_{1s} = 0 \\ A_{2s} = 0 \end{matrix}\right\} \; s = 2f+1, 2f+2, \ldots, 2f+n-1, \quad \begin{matrix} A_{1(2f+n)} = -l_t\cos\beta_1, \\ A_{2(2f+n)} = -l_t\cos\beta_2. \end{matrix} \tag{34}$$

Applying Eq. (32), the $2f$ equations for the span generalized co-ordinates are

$$\begin{aligned} \ddot{a}_r - \frac{\gamma}{l_{i-1}}\textstyle\sum_{s=1}^{f} G_{rs}^{span}\dot{a}_s + \frac{P_{i-1}-\gamma^2}{l_{i-1}^2}\sum_{s=1}^{f} K_{rs}^{span} a_s &= \lambda_1 A_{1r} + \lambda_2 A_{2r} \\ \ddot{b}_r - \frac{\gamma}{l_i}\textstyle\sum_{s=1}^{f} G_{rs}^{span}\dot{b}_s + \frac{P_i-\gamma^2}{l_i^2}\sum_{s=1}^{f} K_{rs}^{span} b_s &= \lambda_1 A_{1(f+r)} + \lambda_2 A_{2(f+r)}, \quad r = 1, 2, \ldots, f. \end{aligned} \tag{35}$$

$$G_{rs}^{span} = \int_0^1 \left(\eta_r\frac{\mathrm{d}\eta_s}{\mathrm{d}\xi} - \eta_s\frac{\mathrm{d}\eta_r}{\mathrm{d}\xi}\right)\mathrm{d}\xi = -G_{rs}^{span}, \quad K_{rs}^{span} = \int_0^1 \frac{\mathrm{d}\eta_r}{\mathrm{d}\xi}\frac{\mathrm{d}\eta_s}{\mathrm{d}\xi}\,\mathrm{d}\xi = K_{rs}^{span}. \tag{36}$$

The equations of motion for the pulley rotations ϕ_j are exactly as in Eqs. (14)–(17). The tensioner equation is given by (18) with two modifications: (1) Eqs. (28) are substituted, and (2) the right-hand side is $\lambda_1(-l_t\cos\beta_1) + \lambda_2(-l_t\cos\beta_2)$. The span Eqs. (35), n equations for the pulleys and tensioner arm, and the two constraints Eq. (33) are put in matrix form as

$$\begin{bmatrix} \mathbf{M}_{11} & 0 \\ 0 & 0 \end{bmatrix}\begin{Bmatrix} \ddot{\mathbf{h}} \\ \ddot{\lambda} \end{Bmatrix} - \begin{bmatrix} \mathbf{G}_{11} & 0 \\ 0 & 0 \end{bmatrix}\begin{Bmatrix} \dot{\mathbf{h}} \\ \dot{\lambda} \end{Bmatrix} + \begin{bmatrix} \mathbf{L}_{11} & \mathbf{L}_{12} \\ \mathbf{L}_{12}^{\mathrm{T}} & 0 \end{bmatrix}\begin{Bmatrix} \mathbf{h} \\ \lambda \end{Bmatrix} = \begin{Bmatrix} \mathbf{f}_1 \\ \mathbf{0} \end{Bmatrix}, \tag{37}$$

$$\mathbf{h} = \left\{ \underbrace{a_1, a_2, \ldots, a_f, b_1, b_2, \ldots, b_f}_{spans}, \underbrace{\phi_2, \phi_3, \ldots, \phi_n, \theta_t}_{pulleys+tensioner} \right\}^{\mathrm{T}}, \quad \lambda = \begin{Bmatrix} \lambda_1 \\ \lambda_2 \end{Bmatrix}, \tag{38}$$

$$\mathbf{M}_{11}=\begin{bmatrix}\mathbf{I}_{fxf} & \mathbf{0} & \mathbf{0} & 0\\ \mathbf{0} & \mathbf{I}_{fxf} & \mathbf{0} & 0\\ \mathbf{0} & \mathbf{0} & diag(J_j) & 0\\ 0 & 0 & 0 & J_t\end{bmatrix},\quad \mathbf{G}_{11}=\gamma\begin{bmatrix}(1/l_{i-1})\mathbf{G}^{span} & \mathbf{0} & \mathbf{0} & \mathbf{0}\\ \mathbf{0} & (1/l_i)\mathbf{G}^{span} & \mathbf{0} & \mathbf{0}\\ \mathbf{0} & \mathbf{0} & \mathbf{0} & \mathbf{0}\\ \mathbf{G}^{t(i-1)} & \mathbf{G}^{t(i)} & \mathbf{0} & 0\end{bmatrix},$$

$$\mathbf{L}_{11}=\begin{bmatrix}\dfrac{P_{i-1}-\gamma^2}{l_{i-1}^2}\mathbf{K}^{span} & \mathbf{0} & \mathbf{0} & \mathbf{0}\\ \mathbf{0} & \dfrac{P_i-\gamma^2}{l_i^2}\mathbf{K}^{span} & \mathbf{0} & \mathbf{0}\\ \mathbf{0} & \mathbf{0} & \mathbf{K}^{pulley} & \mathbf{K}^{pt}\\ \mathbf{K}^{t(i-1)} & \mathbf{K}^{t(i)} & \mathbf{K}^{tp} & K^{tt}\end{bmatrix},\quad \mathbf{L}_{12}=\begin{bmatrix}A_{11} & A_{21}\\ A_{12} & A_{22}\\ \vdots & \vdots\\ A_{1(n+2f)} & A_{2(n+2f)}\end{bmatrix},$$

$$\mathbf{f}_1=\left\{\underbrace{0,\ldots,0}_{2f},J_2\ddot{\theta}_1-M_2,J_3\ddot{\theta}_1-M_3,\ldots,J_n\ddot{\theta}_1-M_n,0\right\}^{\mathrm{T}}, \tag{39}$$

where the components of $\mathbf{G}^{span}$ and $\mathbf{K}^{span}$ are in Eq. (36) and other matrix elements are given in Appendix A.

From Eq. (37),

$$\mathbf{M}_{11}\ddot{\mathbf{h}}-\mathbf{G}_{11}\dot{\mathbf{h}}+\mathbf{L}_{11}\mathbf{h}+\mathbf{L}_{12}\lambda=\mathbf{f}_1. \tag{40}$$

λ can be eliminated by premultiplying Eq. (40) by $\mathbf{C}^{\mathrm{T}}$, where $\mathbf{C}$ is such that $\boldsymbol{C}^{\mathrm{T}}\boldsymbol{L}_{12}=0$ Mathematically, one needs the columns of $\mathbf{C}$ to be a basis for the null space of $\mathbf{L}_{12}^{\mathrm{T}}$. $\mathbf{C}$ is obtained from the singular value decomposition $\mathbf{L}_{12}=\mathbf{U}_{(n+2f)x(n+2f)}\sigma_{(n+2f)x2}\mathbf{V}_{2x2}^{\mathrm{T}}$. $\mathbf{U}$ and $\mathbf{V}$ consist of orthonormal columns such that $\mathbf{U}^{\mathrm{T}}\mathbf{U}=\mathbf{V}^{\mathrm{T}}\mathbf{V}=1$. The rank of $\mathbf{L}_{12}$ is two, and the two non-zero singular values of $\mathbf{L}_{12}$ lie along the main diagonal of σ. The columns of $\mathbf{U}$ corresponding to the $n+2f-2$ zero singular values form the $(n+2f)\times(n+2f-2)$ matrix $\mathbf{C}$. Making the substitution $\mathbf{h}=\mathbf{C}\mathbf{z}$ in Eq. (40) and premultiplying by $\mathbf{C}^{\mathrm{T}}$ leads to

$$\begin{gathered}\mathbf{M}_{system}\ddot{\mathbf{z}}-\mathbf{G}_{system}\dot{\mathbf{z}}+\mathbf{L}_{system}\mathbf{z}=\mathbf{C}^{\mathrm{T}}\mathbf{f}_1=\mathbf{p},\\ \mathbf{M}_{system}=\mathbf{C}^{\mathrm{T}}\mathbf{M}_{11}\mathbf{C},\quad \mathbf{G}_{system}=\mathbf{C}^{\mathrm{T}}\mathbf{G}_{\mathbf{11}}\mathbf{C},\quad \mathbf{L}_{system}=\mathbf{C}^{\mathrm{T}}\mathbf{L}_{11}\mathbf{C}.\end{gathered} \tag{41}$$

This is the final discretized form from which the dynamic response to engine and accessory excitations is calculated. One can readily add modal damping to represent tensioner pivot, belt, and bearing losses.

With the separable form $\mathbf{z}\rightarrow\mathbf{z}\mathrm{e}^{\mathrm{i}\omega t}$, the eigenvalue problem is

$$(-\omega^2\mathbf{M}_{system}-\mathrm{i}\omega\mathbf{G}_{system}+\mathbf{L}_{system})\mathbf{z}=\mathbf{0}. \tag{42}$$

The system modes $\mathbf{h}$ are obtained using $\mathbf{h}=\mathbf{C}\mathbf{z}$; span modal deflections are found from $\mathbf{h}$ and Eq. (28). The convergence and speed improvements over prior methods are discussed later.

4. Calculation of eigensensitivities

Knowledge about the sensitivity of the natural frequencies and vibration modes to the various system parameters informs a designer how to tune natural frequencies away from resonant conditions, which is a common need in vehicle applications. The extended operator representation of the hybrid discrete-continuous model defined by Eqs. (11)–(18) is used in a perturbation analysis to obtain closed-form expressions for the sensitivities.

Perturbing a generic parameter κ of the system by an amount ε from the nominal value κ_0 leads to perturbations of the extended operators in Eq. (27) as

$$L = L_0 + \varepsilon L', \quad G = G_0 + \varepsilon G', \quad M = M_0 + \varepsilon M', \tag{43}$$

where $L' = \partial L/\partial\kappa\big|_{\kappa=\kappa_0}$, etc. The eigensolutions are expressed to first order in ε as

$$\begin{gathered}\omega^2 = \omega_0^2 + \varepsilon\mu, \quad a = a_0 + \varepsilon a_1, \\ \mu = \left.\frac{\partial(\omega^2)}{\partial\kappa}\right|_{\kappa=\kappa_0}, a_1 = \left.\frac{\partial a}{\partial\kappa}\right|_{\kappa=\kappa_0},\end{gathered} \tag{44}$$

where (ω_0^2, a_0) is an eigensolution for $\kappa = \kappa_0$, and a is the extended variable defined in Eq. (19). Substitution of Eqs. (43) and (44) into Eqs. (27) yields

$$L_0 a_0 - \mathrm{i}\omega_0 G_0 a_0 - \omega_0^2 M_0 a_0 = 0, \tag{45}$$

$$L_0 a_1 - \mathrm{i}\omega_0 G_0 a_1 - \omega_0^2 M_0 a_1 = -L' a_0 + \mathrm{i}\omega_0 G' a_0 + \mathrm{i}\frac{\mu}{2\omega_0} G_0 a_0 + \omega_0^2 M' a_0 + \mu M_0 a_0. \tag{46}$$

With the unperturbed eigensolution determined from Eq. (45), the solvability condition for Eq. (46) is

$$\mu = 2\omega_0 \frac{\langle a_0, L' a_0 \rangle + \mathrm{i}\omega_0 \langle a_0, G' a_0 \rangle - \omega_0^2 \langle a_0, M' a_0 \rangle}{2\omega_0 - \mathrm{i}\langle a_0, G_0 a_0 \rangle}, \tag{47}$$

where a_0 is normalized such that $\langle a_0, M_0 a_0 \rangle = 1$. Extension to second order of perturbation is straightforward.

Subsequent sensitivity results are conveniently represented in terms of modal energies. Modal strain energy is given by Eq. (31) with $(\bullet)^2 = |\bullet|^2$. Modal kinetic energy is expressed as

$$T_{modal} = \sum_{j=2}^{n} T_j + T_t + T_{span}^{(2)} + T_{span}^{(1)} + T_{span}^{(0)}, \tag{48}$$

$$\begin{gathered}T_j = 1/2\omega_0^2 J_j |\phi_j|^2, \quad T_t = 1/2\omega_0^2 J_t |\theta_t|^2, \\ T_{span}^{(2)} = \textstyle\sum_{s=i-1}^{i} \dfrac{\omega_0^2}{2} \int_0^{l_s} |w_s|^2 \,\mathrm{d}x_s, \\ T_{span}^{(1)} = -\dfrac{\mathrm{i}\omega_0\gamma}{2} \textstyle\sum_{s=i-1}^{i} \int_0^{l_s} \left(w_s \dfrac{\mathrm{d}\bar{w}_s}{\mathrm{d}x_s} - \bar{w}_s \dfrac{\mathrm{d}w_s}{\mathrm{d}x_s} \right) \mathrm{d}x_s, \\ T_{span}^{(0)} = \gamma^2 \textstyle\sum_{s=i-1}^{i} \dfrac{1}{2} \int_0^{l_s} \left| \dfrac{\mathrm{d}w_s}{\mathrm{d}x_s} \right|^2 \mathrm{d}x_s,\end{gathered}$$

where the eigensolutions are complex for non-zero belt velocity.

Table 1
Natural frequency sensitivities in terms of modal energies

Model parameter	Dimensionless parameter	Natural frequency sensitivity, $\partial(\omega^2)/\partial\kappa$	Mode type most affected
Longitudinal stiffness	$k_b = EA/\hat{P}_1$	$\frac{2\omega_0^2}{k_b}\frac{V_{stretch}}{\omega_0^2 + T_{span}^{(1)}}$	Rotational modes
Tensioner stiffness	k_t	$\frac{2\omega_0^2}{k_t}\frac{V_t}{\omega_0^2 + T_{span}^{(1)}}$	Both types of modes
Static tension	P_{i-1} or P_i	$\frac{2\omega_0^2}{P_{i-1,i}}\frac{V_{span}^{i-1,i}}{\omega_0^2 + T_{span}^{(1)}}$	Transverse belt modes
Speed	γ	$\frac{-2\omega_0^2}{\gamma}\frac{T_{span}^{(1)} + 2T_{span}^{(0)}}{\omega_0^2 + T_{span}^{(1)}}$	Transverse belt modes
Pulley moments of inertia	J_j	$\frac{-2\omega_0^2}{J_j}\frac{T_j}{\omega_0^2 + T_{span}^{(1)}}$	Rotational modes
Tensioner moment of inertia	J_t	$\frac{-2\omega_0^2}{J_t}\frac{T_t}{\omega_0^2 + T_{span}^{(1)}}$	Both types of modes

For the purpose of illustration, choose κ=k_b as the parameter to be varied. This gives$L' = \partial L/\partial k_b$, $M' = G' = 0$. Using Eqs. (47), (31) and (48), the sensitivity to k_b is

$$\mu = \frac{\partial\omega^2}{\partial k_b} = \frac{2\omega_0^2}{k_b}\frac{V_{stretch}}{\omega_0^2 + T_{span}^{(1)}}. \tag{49}$$

A similar technique is applied to find sensitivities to other system parameters in terms of modal energies. The results are listed in Table 1. Dimensional sensitivities are related to the dimensionless ones by

$$\frac{\partial(\hat{\omega}^2)}{\partial\hat{\kappa}} = \frac{\hat{P}_1}{\hat{\rho}\hat{l}_1^2\sigma}\frac{\partial(\omega^2)}{\partial\kappa},$$

where the parameters are related by $\hat{\kappa} = \sigma\kappa$. Also,

$$\frac{\partial\omega}{\partial\kappa} = \frac{1}{2\omega}\frac{\partial(\omega^2)}{\partial\kappa}, \quad \frac{\partial\hat{\omega}}{\partial\hat{\kappa}} = \frac{1}{2\hat{\omega}}\frac{\partial(\hat{\omega}^2)}{\partial\hat{\kappa}}.$$

These results show that the eigenvalue sensitivities to stiffness and inertia parameters are directly related to the modal strain and kinetic energy distribution. This allows one to analyze the sensitivities qualitatively and quantitatively by examining modal energy charts. Using Table 1, the sensitivity of a particular mode to stiffness and mass parameter changes is immediately clear from a single modal strain/kinetic energy distribution chart such as those shown in Fig. 4(b) and Fig. 5(b). Because $\gamma = 0$ in these figures, the span modal kinetic energies are solely from $T_{span}^{(2)}$. Notice that sensitivity μ of a given natural frequency to *any* parameter change is obtained by inspection of a *single* modal strain/kinetic energy chart, making it a practical tool for rapid

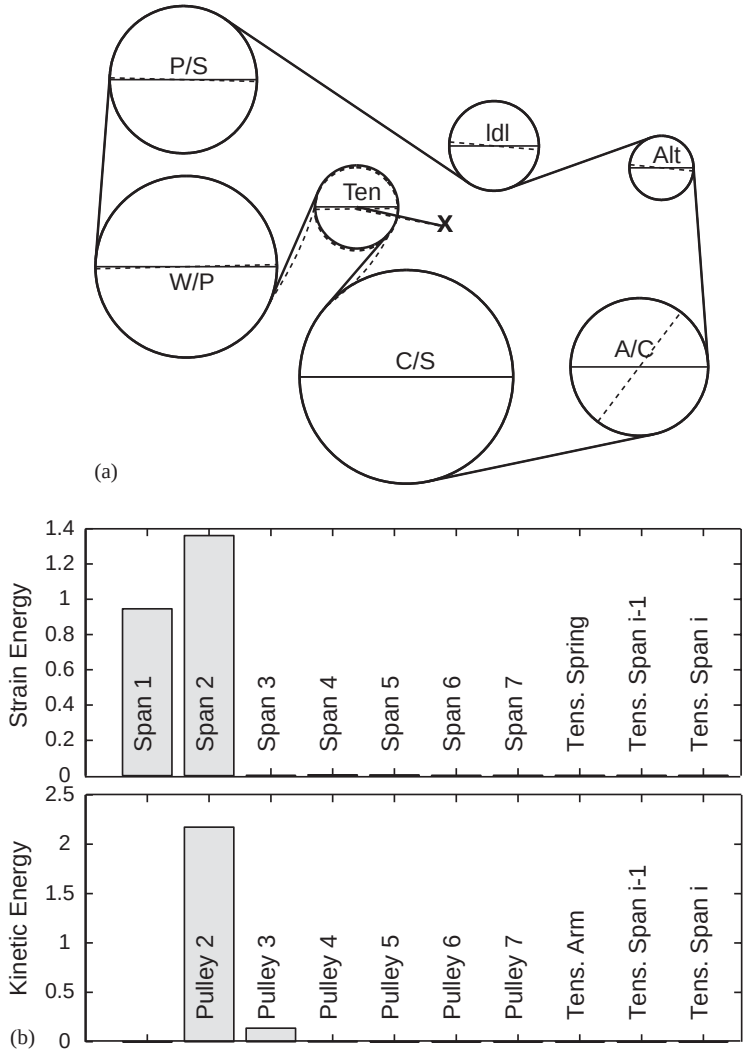

Fig. 4. (a) Vibration mode 3 ($\omega_3 = 2.151$) for nominal values of parameters from Table 2. The belt speed is zero. (b) Dimensionless modal energy diagram for mode 3.

sensitivity assessments. Eigensolution changes from multiple parameter variations ε_j are determined by

$$\omega^2 = \omega_0^2 + \sum_{j=1}^{m} \varepsilon_j \mu_j, \tag{50}$$

where each μ_j is calculated as above.

The above eigensensitivity results are applicable to continuum eigensolutions. For the discretized system, the following energy expressions can be used directly with the expressions in

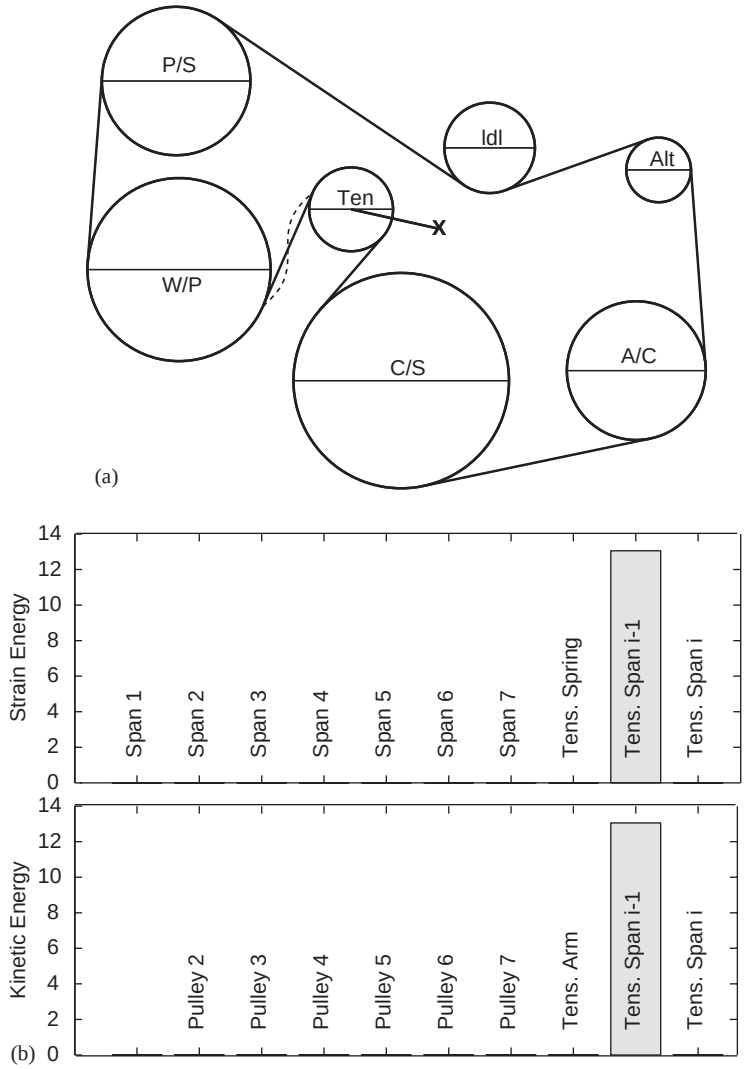

Fig. 5. (a) Vibration mode 8 ($\omega_8 = 5.109$) for nominal values of parameters from Table 2. The belt speed is zero. (b) Dimensionless modal energy diagram for mode 8.

Table 1 to compute sensitivities of the discretized model:

$$T_{modal} = \sum_{j=2}^{n} T_j + T_t + T_{span}^{(2)} + T_{span}^{(1)} + T_{span}^{(0)}, \quad T_j = 1/2\omega_0^2 J_j |\phi_j|^2,$$

$$T_t = 1/2\omega_0^2 J_t |\phi_t|^2, \quad T_{span}^{(2)} = \frac{\omega_0^2}{2}(\mathbf{a}^{\mathrm{T}}\bar{\mathbf{a}} + \mathbf{b}^{\mathrm{T}}\bar{\mathbf{b}}),$$

$$T_{span}^{(1)} = -\frac{\mathrm{i}\omega_0\gamma}{2}[(1/l_{i-1})\mathbf{a}^{\mathrm{T}}\mathbf{G}^{span}\bar{\mathbf{a}} + (1/l_i)\mathbf{b}^{\mathrm{T}}\mathbf{G}^{span}\bar{\mathbf{b}}],$$

$$T_{span}^{(0)} = \frac{\gamma^2}{2}[(1/l_{i-1}^2)\mathbf{a}^{\mathrm{T}}\mathbf{K}^{span}\bar{\mathbf{a}} + (1/l_{i-1}^2)\mathbf{b}^{\mathrm{T}}\mathbf{K}^{span}\bar{\mathbf{b}}], \tag{51}$$

Table 2
Parameters of an example system with seven pulleys

Number of pulleys	7
Tensioner pulley number	7
Belt tensile modulus, EA (N)	111,200
Belt density, $\hat{\rho}$ (kg/m)	0.107

Pulley number	Pulley name	X coord. (mm)	Y coord. (mm)	Diameter (mm)	$\hat{J}_j$ (kg m^2)	Steady torque (N m)
1	C/S	0	0	194	0.122	
2	A/C	211.6	9	125	0.003785	−24.820
3	ALT	231.7	189.8	58.2	0.0043	−9.090
4	Idler	79.6	209.7	81.5	0.00024	0
5	P/S	−202.6	269.9	133.7	0.000596	−18.908
6	W/P	−200	100	164.9	0.004596	−2.382
7	Ten	−45.1	154.3	75.5	0.000043	0

Tensioner Pivot X coord. (mm)	Pivot Y coord. (mm)	$\hat{J}_t$ (kg m^2)	Initial torque (N m)	$\hat{K}_t$ (N m/rad)
33	137	0.004601	39.768	38.84

$$V = \sum_{j=1 j\neq i-1,i}^{n} \frac{1}{2}\frac{k_b}{l_j}|\phi_{j+1} - \phi_j|^2 + \frac{1}{2}\frac{k_b}{l_{i-1}}|\phi_i - \phi_{i-1} - l_t\theta_t \sin\beta_1|^2 + \frac{1}{2}\frac{k_b}{l_i}|\phi_{i+1} - \phi_i + l_t\theta_t \sin\beta_2|^2 + \frac{1}{2}k_t l_t^2|\theta_t|^2 + \frac{P_{i-1}}{l_{i-1}^2}\mathbf{a}^{\mathrm{T}}\mathbf{K}^{span}\bar{\mathbf{a}} + \frac{P_i}{l_i^2}\mathbf{b}^{\mathrm{T}}\mathbf{K}^{span}\bar{\mathbf{b}} = V_{stretch} + V_t + V_{span}^{i-1} + V_{span}^{i}, \quad (52)$$

where $\mathbf{a}$ and $\mathbf{b}$ are sub-vectors drawn from Eq. (38) and the vibration modes are normalized according to $\mathbf{h}^{\mathrm{T}}\mathbf{M}_{11}\bar{\mathbf{h}} = 1$ which is derived from $\langle a_0, M_0 a_0 \rangle = 1$.

5. Results

The foregoing analysis was formulated in a general purpose program and applied to a current automobile experiencing a vibration and noise problem (Fig. 1). The nominal system parameters are listed in Table 2 with corresponding equilibrium span tensions, span lengths, and tensioner orientation in Table 3. Table 4 gives the natural frequencies and vibration modes for the nominal system parameters. The modes are either predominantly *rotational modes* with pulley and tensioner rotation but little span motion (Fig. 4) or *belt modes* having mostly transverse motion of the tensioner spans with little pulley rotation (Fig. 5).

Table 3
Equilibrium span tensions, span lengths, and tensioner orientation for the example system in Table 2 and a crank-shaft speed of 680 r.p.m., corresponding to a belt speed of $\hat{\gamma} = 6.907$ m/s. From Eq. (10), the dimensionless speed is $\gamma = 0.0632$

Span	1	2	3	4	5	6	7
Tension (N)	1278.	881.1	568.7	568.7	285.9	257.0	257.0
Length (mm)	209.0	178.8	136.6	267.7	169.2	114.4	92.71
Tensioner equilibrium	$\theta_{tr} = 165.2^\circ$		$\beta_1 = 98.52^\circ$		$\beta_2 = -65.06^\circ$		

Table 4
Dimensionless and dimensional natural frequencies of the example in Table 2 and a crank-shaft speed of 680 r.p.m., corresponding to a belt speed of $\hat{\gamma} = 6.907$ m/s. From Eq. (10), the dimensionless speed is $\gamma = 0.0632$. $\hat{P}_1, \hat{\rho}, \hat{l}_1$ are given in Tables 2 and 3

Mode	Non-dimensional natural frequency, ω	Dimensional natural frequency (Hz) $\hat{f} = \frac{\omega}{2\pi}\sqrt{\hat{P}_1/(\hat{\rho}\hat{l}_1^2)}$	Mode description
1	0.3947	32.85	1st rotational mode
2	0.9550	79.48	2nd rotational mode
3	2.147	178.7	3rd rotational mode
4	2.522	210.0	1st transverse mode, span 6
5	3.111	258.9	1st transverse mode, span 7
6	3.509	292.0	4th rotational mode
7	4.685	389.9	5th rotational mode
8	5.047	420.0	2nd transverse mode, span 6
9	6.227	518.2	2nd transverse mode, span 7
10	6.501	541.0	6th rotational mode

The speed improvements are striking. For this example system, the subroutine for computing the eigenvalues using the presented discretization takes 0.002 s as opposed to 64.2 s for the numerical root finding approach of Ref. [10] over 0–450 Hz. This comparison represents the CPU time in the eigenvalue solution subroutine for both methods executed on the same modern desktop computer. This is an advantage in industrial applications where one routinely conducts free vibration or dynamic response analyses repeatedly for a range of engine speeds or other parameters (e.g., 500–5000 rpm at 10 rpm increments is not unusual). The speed in the root finding approach depends heavily on the frequency search range (which must be estimated by the user) and the resolution in dividing the frequency axis. In implementing the continuum formulations [10,11], we found it necessary to use extreme caution in the numerical subroutine to avoid erroneously missing or duplicating roots. Even then our choices for one system occasionally failed on other systems. Despite considerable effort, we did not find uniformly valid parameters to confidently avoid numerical problems using existing continuum eigenvalue solutions. Numerical robustness is not a concern with the discretization. Neither is accuracy; the calculated eigensolutions are virtually indistinguishable from the continuum formulations. Additionally,

there is no need to specify the frequency range a priori. The convergence of the natural frequencies obtained using different numbers of basis functions per span is shown in Fig. 6.

Figs. 7–9 show natural frequencies for system parameters varying over wide ranges. In Fig. 7, rotational modes (mode 3, for example) are sensitive to longitudinal belt stiffness k_b because their strain energy is concentrated in belt stretching ($V_{stretch}$ in Eqs. (31) and (52)). Belt modes (for example, mode 8) are not significantly affected by k_b except for very low values. Fig. 8, where belt density is the changing parameter demonstrates a converse relationship: belt modes are significantly affected while rotational modes are only affected slightly. The modes affected by changing a particular parameter can be even more restricted. For example, only those modes with significant modal kinetic energy in a given pulley respond to changes in that pulley inertia. Fig. 9

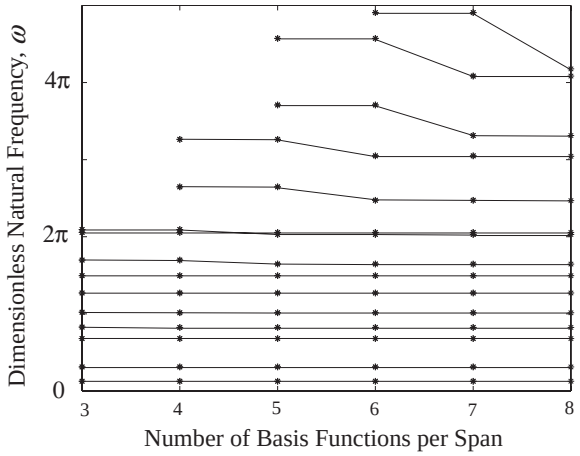

Fig. 6. Convergence of dimensionless natural frequencies for increasing number of basis functions per span. Parameters are from Table 2. The belt speed is zero.

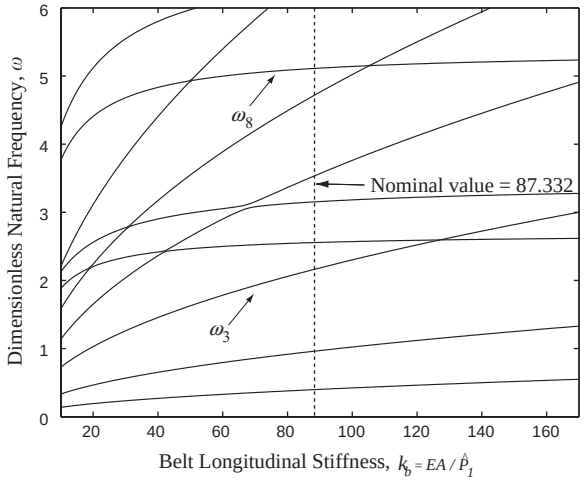

Fig. 7. Variation of natural frequencies with $k_b = EA/\hat{P}_1$ for nominal values of system parameters as given in Table 2. The belt speed is zero.

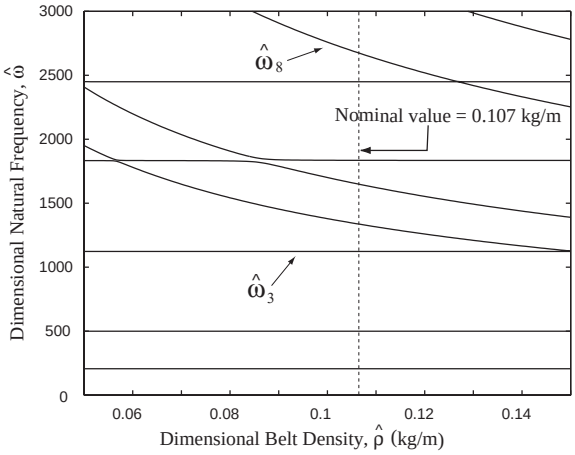

Fig. 8. Variation of natural frequencies with belt density $\hat{\rho}$ for nominal values of system parameters as given in Table 2. The belt speed is zero.

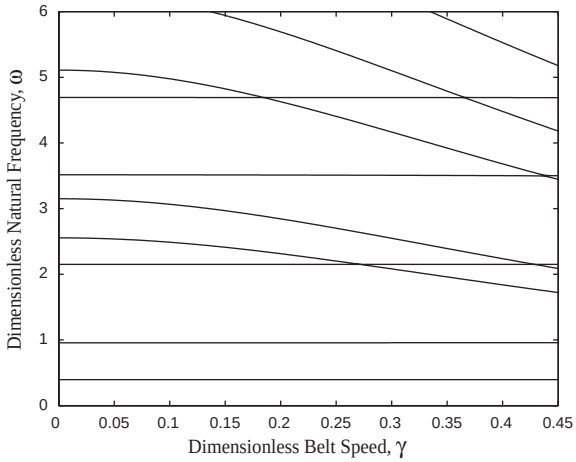

Fig. 9. Variation of natural frequencies with belt speed γ for nominal values of system parameters as given in Table 2.

shows natural frequency dependence on engine (belt) speed. The belt modes are affected most, with each one decreasing monotonically. Although typical vehicle speeds are well below any critical speeds, speed variations across the typical vehicle engine speed range can cause significant changes in natural frequency ($\approx$20–40%) and vibration modes. Gyroscopic effects are not negligible in practical high-speed engine regimes. The slopes of the presented natural frequency curves at any point are calculable directly from Table 1 and modal energy charts. Qualitative results are clear from the modal energy charts.

Note that eigenvalue veering occurs in the natural frequency plots (Fig. 8 near $\hat{\rho} = 0.085$ and Fig. 7, for example). This is characterized by two eigenvalue loci approaching each other but then repelling away as a parameter varies across a range. The eigenvalue veering persists even if very

small parameter increments are used. The veering modes are strongly coupled in the veering region. The modes undergo large changes for parameter variations in this neighborhood, with the sharpness of the veering dictating the extent of the modal coupling and sharpness of the modal changes. From a practical viewpoint, this has implications for the dynamic response. Small parameter changes (or uncertainties) can lead to markedly different modes and so markedly different dynamic response under operating conditions.

The rotational modes have large pulley rotation and high strain energy due to belt stretching. Thus, these modes will be sensitive to changes in longitudinal belt stiffness, pulley inertia, and tensioner inertia. They are relatively insensitive to belt tension, belt density, and speed. Conversely, the belt modes are sensitive to changes in belt tension, speed, and density. They are considerably less sensitive to belt longitudinal stiffness and pulley inertia. Both mode types can involve tensioner motion, and so both are sensitive to tensioner pivot stiffness. The last column of Table 1 summarizes these findings. Of course, coupled modes that do not fall obviously into either of these categories are possible, especially in regions of eigenvalue veering.

The concepts presented in this work were applied to investigate a troublesome vibration and noise problem experienced by this vehicle. A sustained, audible noise resulting from large motion of the air conditioner-alternator span occurred near engine idle speed when the air conditioner was turned on. Experiments were conducted on a full-size belt drive test stand. The drive was mounted on a heavy, fixed frame. To faithfully represent the system, the vehicle engine drove the system with actual vehicle accessories attached to load banks that duplicate the in-vehicle characteristics. Sensors measured the pulley and tensioner rotational oscillations. When the air conditioner is turned on, the crank-shaft speed drops and experiences significant speed fluctuations, inducing vibration of the system at the frequency of the crank-shaft fluctuations (Fig. 10). The mean crank-shaft speed of 680 rpm corresponds to a belt speed of $\hat{\gamma} = 6.907\,\mathrm{m/s}$ and an engine firing frequency of 34 Hz for this six-cylinder engine (three firings per crank-shaft

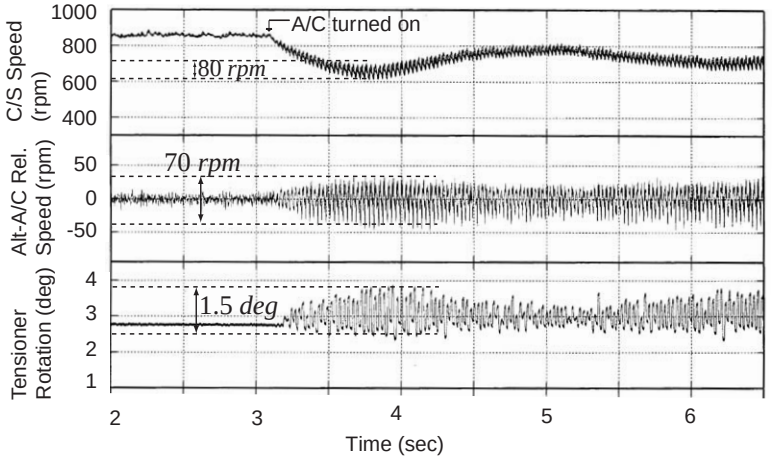

Fig. 10. Experimentally measured dynamic response of system of Table 2. The amplitudes are: crank-shaft speed = 80 rpm, alternator-air conditioner relative speed $\dot{\theta}_3 - \dot{\theta}_2 = 70$ r.p.m., and tensioner rotation $\dot{\theta}_t = 1.5°$.

revolution). This is the frequency of the crank-shaft speed fluctuations that excite the system (see Eqs. (14)–(17), (25) and (39)). The measured relative speed between the alternator and air conditioner pulleys ($\dot{\theta}_3 - \dot{\theta}_2$) and the tensioner rotation $\dot{\theta}_t$ are given in Fig. 10. The equilibrium tensions, span lengths, and tensioner orientation for this speed are given in Table 3, and the natural frequencies are given in Table 4. Using the estimated crank-shaft speed fluctuations of 80 rpm peak–peak at a frequency of 34 Hz, the steady state dynamic response of the system was predicted using Eq. (41) and modal damping of 8%. The analytically calculated amplitude of alternator-air conditioner relative speed is 68 rpm, a difference of a few percent with the experimental estimate of 70 rpm. The analytically calculated tensioner rotation amplitude is 1.6°, again within a few percent of the experimental estimate of 1.5°. The source of the vibration problem is that the first belt drive natural frequency of 32.85 Hz (Table 4) nearly coincides with the dominant excitation near 34 Hz. The corresponding mode has large relative rotation between the alternator and air conditioner, and large response in this mode drives the troublesome motion of the adjoining span. Expanded modeling that captures pulley-belt span coupling between *fixed-center* pulleys, due to bending stiffness, for example Refs. [16,17], is required to obtain *quantitative* predictions of the air conditioner-alternator *span* response. The eigensensitivity results were used to identify effective means to tune this natural frequency away from the excitation frequency. Implementation of the changes altered the natural frequency and resolved the problem.

6. Summary and conclusions

(1) This work finds an efficient and accurate method to calculate the natural frequencies, vibration modes, and dynamic response of a serpentine belt-drive system. The method relies on spatial discretization of the belt spans with Lagrange multipliers imposing the geometric boundary conditions. This approach is several orders of magnitude faster than previously published methods and is not subject to the robustness problems present in these methods. No sacrifice in accuracy is made in this process. The formulation is amenable to writing general-purpose codes.

(2) Eigenvalue perturbation of a mathematically structured form of the discrete-continuous model leads to simple, closed-form expressions for the natural frequency sensitivity to belt drive parameters. These sensitivities aid the common process of natural frequency tuning to troubleshoot practical vehicle vibration problems. They are also a tool to assess the impact of multiple design choices on dynamic characteristics.

(3) The vibration modes for typical parameter ranges divide approximately into two categories: *rotational* modes with dominantly pulley and tensioner rotation (with little transverse belt motion) and *belt* modes with predominantly transverse motion of the spans adjacent to the tensioner (and little pulley motion). These mode types show markedly different, and complementary, sensitivities to system parameters.

(4) Natural frequency sensitivity is closely related to the modal strain and kinetic energies. A single modal energy diagram efficiently expresses the sensitivity of a given mode to *all* stiffness and inertia parameters. Qualitative sensitivity is clear by inspection; quantitative values are obtained from Table 1.

Acknowledgements

Thanks are due to Mark IV Automotive/Dayco Corporation for support of this project and for the experimental data. Thanks also to Mr. Lingyuan Kong and Mr. Shrenik Shah for help in verifying the analysis and generating numerical results.

Appendix A. Elements of matrices in Eq. (37)

$$\mathbf{G}^{t(i-1)} = l_t \cos\beta_1[\alpha_1(1), \alpha_2(1), \ldots, \alpha_f(1)],$$

$$\mathbf{G}^{t(i)} = -l_t \cos\beta_2[\psi_1(0), \psi_2(0), , \ldots, \psi_f(0)],$$

$$\mathbf{K}^{t(i-1)} = (l_t/l_{i-1})(P_{i-1} - \gamma^2)\cos\beta_1[\alpha_1'(1), \alpha_2'(1), \ldots, \alpha_f'(1)],$$

$$\mathbf{K}^{t(i)} = -(l_t/l_i)(P_i - \gamma^2)\cos\beta_2[\psi_1'(0), \psi_2'(0), , \ldots, \psi_f'(0)],$$

$$K^{tt} = l_t^2\left(k_t + \frac{k_b}{l_{i-1}}\sin^2\beta_1 + \frac{k_b}{l_i}\sin^2\beta_2\right),$$

$$\mathbf{K}^{tp}(1, i-2) = l_t(k_b/l_{i-1})\sin\beta_1,$$

$$\mathbf{K}^{tp}(1, i-1) = -l_t[(k_b/l_{i-1})\sin\beta_1 + (k_b/l_i)\sin\beta_2],$$

$$\mathbf{K}^{tp}(1, i) = l_t(k_b/l_i)\sin\beta_2.$$

Note that other elements of $\mathbf{K}^{tp}$ are zero and $\mathbf{K}^{pt} = transpose(\mathbf{K}^{tp})$.

$$\mathbf{K}^{pulley}(m, m-1) = -\frac{k_b}{l_m},\ \ \mathbf{K}^{pulley}(m, m) = \frac{k_b}{l_m} + \frac{k_b}{l_{m+1}},\ \ \mathbf{K}^{pulley}(m, m+1) = -\frac{k_b}{l_{m+1}},$$

where $m = 1, 2, \ldots, n-1$. All elements in $\mathbf{K}^{pulley}$ other than the above are zero.

References

[1] L.E. Hawker, A Vibration Analysis of Automotive Serpentine Accessory Drives Systems, Ph.D. Dissertation, University of Windsor, Ontario, Canada, 1991.
[2] C.R. Barker, L.R. Oliver, W.F. Breig, Dynamic Analysis of Belt Drive Tension Forces During Rapid Engine Acceleration, SAE Paper No. 910687, 1991.
[3] S.J. Hwang, N.C. Perkins, A.G. Ulsoy, R. Meckstroth, Rotational response and slip prediction of serpentine belt drives systems, Journal of Vibration Acoustics 17 (1994) 71–78.
[4] T.C. Kraver, G.W. Fan, J.J. Shah, Complex modal analysis of a flat belt pulley system with belt damping and Coulomb-damped tensioner, Journal of Mechanical Design 118 (1996) 306–311.
[5] S. Abrate, Vibrations of belts and belt drives, Mechanism and Machine Theory 27 (1992) 645–659.
[6] A.G. Ulsoy, J.E. Whitesell, M.D. Hooven, Design of belt-tensioner systems for dynamic stability, Journal of Vibrations Acoustics Stress and Reliability in Design 107 (1985) 282–290.

[7] E.M. Mockensturm, N.C. Perkins, A.G. Ulsoy, Stability and limit cycles of parametrically excited, axially moving strings, Journal of Vibration and Acoustics 118 (1996) 346–351.
[8] R.G. Parker, Y. Lin, Parametric instability of axially moving media subjected to multifrequency tension and speed fluctuations, Journal of Applied Mechanics 68 (2001) 49–57.
[9] M. Pakdemirli, A.G. Ulsoy, Stability analysis of an axially accelerating string, Journal of Sound and Vibration 203 (1997) 815–832.
[10] R.S. Beikmann, N.C. Perkins, A.G. Ulsoy, Free vibration of serpentine belt drive systems, Journal of Vibration and Acoustics 118 (1996) 406–413.
[11] L. Zhang, J.W. Zu, Modal analysis of serpentine belt drive systems, Journal of Sound and Vibration 222 (1999) 259–279.
[12] R.S. Beikmann, N.C. Perkins, A.G. Ulsoy, Design and analysis of automotive serpentine belt drive systems for steady state performance, Journal of Mechanical Design 119 (1997) 162–168.
[13] R.S. Beikmann, N.C. Perkins, A.G. Ulsoy, Nonlinear coupled vibration response of serpentine belt drive dynamics, Journal of Vibration and Acoustics 118 (1996) 567–574.
[14] R.G. Parker, Analytical vibration of spinning, elastic disk-spindle systems, Journal of Applied Mechanics 66 (1999) 218–224.
[15] R.G. Parker, C.D. Mote Jr., Vibration and coupling phenomena in asymmetric disk-spindle systems, Journal of Applied Mechanics 63 (1996) 953–961.
[16] L. Kong, R.G. Parker, Equilibrium and belt-pulley vibration coupling in serpentine belt drives, Journal of Applied Mechanics 70 (2003) 739–750.
[17] L. Kong, R.G. Parker, Coupled belt-pulley vibration in serpentine drives with belt bending stiffness, Journal of Applied Mechanics, submitted for publication.